

Article

Synthesis, Characterization of Some Conductive Aromatic Polyamides/Fe₃O₄ NPs/ITO, and Their Utilization for Methotrexate Sensing

Mona A. Abdel-Rahman *, Waleed A. El-Said * , Eman M. Sayed and Aboel-Magd A. Abdel-Wahab

Chemistry Department, Faculty of Science, Assiut University, Assiut 71516, Egypt

* Correspondence: mona.ali1@aun.edu.eg (M.A.A.-R.); awaleedahmed@yahoo.com (W.A.E.-S.)

Abstract: Here, we have synthesized four series of polyamide-conductive polymers and used them to modify Fe₃O₄ NPs/ITO electrodes. The ability of the modified electrodes to detect methotrexate (MTX) anticancer drug electrochemically was investigated. Synthesis of the target-conducting polyamides, P1a–d, P2a–d, P3a, P3b, P3d, and P4c–d, based on different aromatic moieties, such as ethyl 4-(2-(4H-pyrazol-4-ylidene)hydrazinyl)benzoate, diphenyl sulfone, diphenyl ether or phenyl, has been achieved. They were successfully prepared in good yield via solution–polycondensation reaction of the diamino monomers with different dicarboxylic acid chlorides in the presence of N-methyl-2-pyrrolidone (NMP) as a solvent and anhydrous LiCl as a catalyst. A model compound **4** was synthesized from one mole of ethyl-4-(2-(3, 5-diamino-4H-pyrazol-4-ylidene)hydrazinyl) benzoate (diamino monomer) (**3**) with two moles benzoyl chloride. The structure of the synthesized monomers and polymers was confirmed by elemental and spectral analyses. In addition, thermogravimetric analysis evaluated the thermal stabilities of these polyamides. Furthermore, the morphological properties of selected polyamides were examined using an scanning electron microscope. Polyamide/Fe₃O₄/ITO electrodes were prepared, and the electrochemical measurements were performed to measure the new polyamides' conductivity and to detect the MTX anticancer drug in phosphate buffer saline using cyclic voltammetry. The polyamides (P3b and P4b)/Fe₃O₄/ITO electrodes showed the highest sensitivity and reversibility towards MTX.

Keywords: nanomaterials; methotrexate; conductive polymers; iron oxide nanoparticles



Citation: Abdel-Rahman, M.A.; El-Said, W.A.; Sayed, E.M.; Abdel-Wahab, A.-M.A. Synthesis, Characterization of Some Conductive Aromatic Polyamides/Fe₃O₄ NPs/ITO, and Their Utilization for Methotrexate Sensing. *Surfaces* **2023**, *6*, 83–96. <https://doi.org/10.3390/surfaces6010007>

Academic Editor: Gaetano Granozzi

Received: 16 September 2022

Revised: 24 February 2023

Accepted: 25 February 2023

Published: 3 March 2023



Copyright: © 2023 by the authors. Licensee MDPI, Basel, Switzerland. This article is an open access article distributed under the terms and conditions of the Creative Commons Attribution (CC BY) license (<https://creativecommons.org/licenses/by/4.0/>).

1. Introduction

The realm of chemical analysis has demonstrated extraordinary development, especially in the medicinal and environmental fields. Of special interest is the invention of biosensors. Biosensors are devices used to detect the presence of a biological analyte or a chemical substance that combines biological components with a physicochemical detector [1–3]. Polymers are promising candidates that can facilitate a new generation of biosensors [4–8].

Polyamides are widely used materials due to their important properties and acceptable prices [9]. Aromatic polyamides (aramids) are of great technical interest, as they possess a combination of useful properties such as thermal stability [10–12], ionic conductivity [13], low flammability [14–18], and excellent mechanical properties in the form of fibers and composites [19–22]. The inclusion of ether, sulfide, or sulfone groups into the aromatic polyamides enhances the flexibility of the chain, making it easier to process from the melt and giving better solubility in various organic and inorganic solvents [23]. Moreover, aromatic polyamides containing arylene sulfone arylene ether sulfone linkage are amorphous and have a low glass transition temperature (T_g), tractability, and higher thermal-oxidative stability [24,25]. The synthesis of aromatic polyamides is usually based on the condensation of aromatic diamines or their derivatives with dicarboxylic acid chlorides in aprotic polar solvents, such as dimethylformamide, *N,N*-dimethylacetamide, or

N-methyl pyrrolidone [26]. Some aromatic polyamides containing an azo group exhibiting liquid crystalline behavior have been spun into high-strength, high-modulus fibers [27]. Moreover, the incorporation of the azo group into the main chain of the polymer not only imparts color, but is also promising for optical switching and digital storage [28].

Electrodes modified with different nanomaterials [29–32] and conducting polymers have emerged as an important category of biosensor electrodes [33]. Some of the polyamides are conductive polymers [34], and their conductivity can be increased by composite with other materials, which enhances their electrical properties, such as polyaniline (PANI), carbon nanotubes (CNTs) [35,36], graphene [37], and polycarbonate [38]. Motivated by the promising characteristics of aromatic polyamides, some selected polyamide/Fe₃O₄/ITO electrodes were prepared and tested to detect methotrexate (MTX) in phosphate buffer saline (PBS) and real clinical patient blood serum. The target MTX drug was selected due to its anticancer activity and high toxicity to the cancer cells and to all cells. Of course, the presence of amino groups and carboxylic groups in MTX makes it easily oxidized and reduced electrochemically.

2. Materials and Methods

2.1. Materials

All the prepared polymers are new aramids; details of the synthesis and characterization of monomers, acid chlorides, and polymers are given in the experimental part. Ethyl 4-aminobenzoate (Sigma–Aldrich, 98%), *p*-phenylenediamine (Sigma–Aldrich, ≥99%), 4,4'-diaminodiphenyl sulfone (Sigma–Aldrich, ≥97%), 4,4'-diaminodiphenyl ether (Sigma–Aldrich, ≥97%), malononitrile (Sigma–Aldrich, ≥99%), Terephthalic acid, (Sigma–Aldrich, ≥98%), Isophthalic acid (Sigma–Aldrich, ≥99%) were used; all reactions were monitored by thin-layer chromatography (TLC) using TLC silica gel-coated aluminum plates 60F254 (Merck). Other reagents and solvents were purchased and used as received unless otherwise listed. All reactions were achieved under a nitrogen atmosphere. The acid chlorides 1a–d were prepared according to previous literature [39–41], as shown in supporting information.

2.2. Characterization Techniques

All melting points of monomers, model compounds, and polymers were measured using the MEL-TEMP II laboratory device, USA, instrument (Assiut University). Varo MACRO cube: elemental analyzer/Elementar (Egyptian Petroleum Research Institute, Cairo, Egypt) was used to record elemental analyses of all prepared compounds. Fourier transform infrared (FT-IR) spectra of all prepared materials were recorded by using Nicolet 6700, Thermo Fisher Scientific, USA, spectrophotometer, using the KBr pellet technique (Assiut University, Egypt). The UV-visible spectra were recorded in *N*-methyl-2-pyrrolidone (200–700 nm) using Shimadzu 2110 PC scanning spectrophotometer (Assiut University, Egypt). ¹H NMR spectra were recorded using Bruker High-Performance Digital FT-NMR Spectrometer AVANCE III 400 MHz (Cairo University), Varian EM390 (90 MHz) Spectrometer (Assiut University), and AVANCE-III 400 MHz High-Performance FT-NMR Spectrometer BRUKER-BioSpin International AG-Switzerland (Sohag University, Egypt); the chemical shifts are reported at δ values (ppm) relative to TMS as an internal reference. Mass spectra were performed on Thermo SCIENTIFIC Spectrometer (Assiut University, Egypt) and Electrospray Ionization Mass Spectrometry (ETH Zürich, Switzerland). Thermogravimetric analysis (TGA) was measured under nitrogen using the TGA-50 SHIMADZU instrument (Al-Azhar University, Assiut), at a heating rate of 10 °C/min. The morphologies of selected polyamide samples were examined by scanning electron microscope (SEM) using a Jeol JSM-5400 LV instrument (Assiut University, Egypt). SEM sample was prepared on a copper holder by placing a smooth part of the sample powder and then covering with gold/palladium alloy. SEM images were taken using a Pentax Z-50P Camera with Ilford film at an accelerating voltage of 15 kV, using a low-dose technique.

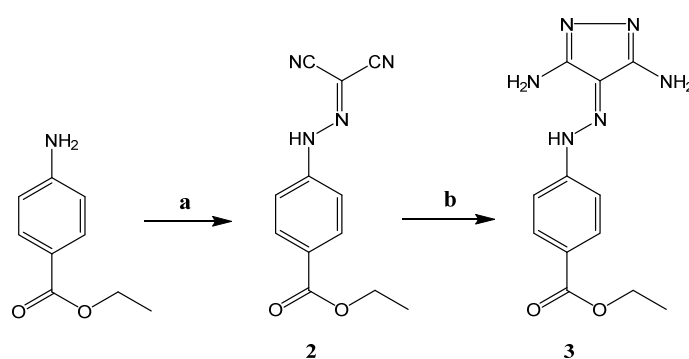
The X-ray diffraction patterns of the polyamides and polyamide/Fe₃O₄/ITO hybrid samples were obtained with X-ray PW 1710 control unit Philips anode material Cu (40 K.V,

30 M.A) Optics in (flex, Holanda): Automatic divergence slit Beta filtering was performed using a graphite monochromator (Assiut University).

2.3. Monomer Synthesis

2.3.1. Synthesis of the Dicyano Compound 2

Sodium nitrite (2.07 g, 30.00 mmol) in 10 mL H₂O was added to ethyl p-aminobenzoate (3.30 g, 20.00 mmol), dissolved in 5 mL dilute HCl. The mixture was cooled to 0 °C and then a solution of malononitrile (2.16 g, 32.72 mmol) in methanol (6 mL) was added dropwise, with stirring for 30 min at −5 °C (Scheme 1-a). A solid product was separated, filtrated off, dried, and recrystallized from methanol as yellow plates; yield: 74.40%; m.p.: 188 °C. Anal. Calcd. for C₁₂H₁₀N₄O₂: C, 59.50; H, 4.16; N, 23.13. Found: C, 59.35; H, 4.59; N, 23.25. FT-IR (KBr, cm^{−1}): 2230 (C≡N) and 1706 (C=O ester). ¹H NMR (400 MHz, CDCl₃): δ = 10.00 (s, 1H, NH), 8.20–7.31 (m, 4H, Ar-H), 4.22–4.70 (q, 2H, CH₂), 1.34 (t, 3H, CH₃). MS: m/z [M⁺] = 243.08 (100%).



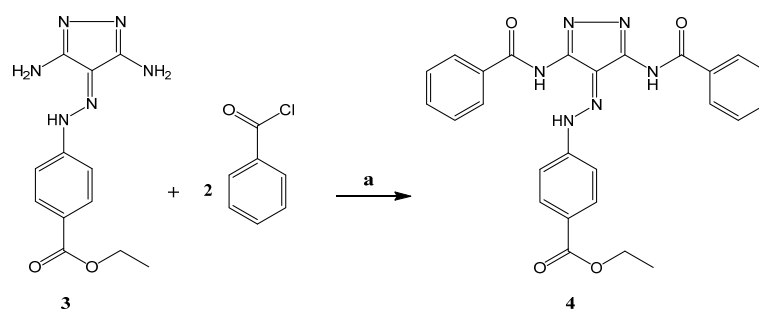
Scheme 1. Synthetic sequence of diamino monomer 3. Reagents and conditions: (a) malononitrile, NaNO₂, HCl, MeOH, stirring, −5 °C; (b) hydrazine hydrate, EtOH, reflux at 70 °C.

2.3.2. Synthesis of the Diamino Monomer 3

A mixture of the dicyano monomer 2 (2.14 g, 8.88 mmol) and hydrazine hydrate (0.50 mL, 9.63 mmol) was dissolved in absolute ethanol (25 mL). The mixture was refluxed for 1 h at 70 °C (Scheme 1-b). A solid product was separated, filtrated off, dried, and recrystallized from ethanol as yellow crystals; yield: 81.7%; m.p: 255 °C. Anal. Calcd. for C₁₂H₁₄N₆O₂: C, 52.55; H, 5.14; N, 30.64. Found: C, 52.16; H, 5.05; N, 30.58. FT-IR (KBr, cm^{−1}): 3392 (NH₂, amine), 1715 (C=O ester). ¹H NMR (400 MHz, DMSO-d₆): δ = 8.20–7.60 (dd, 4H, Ar-H), 4.7–6.00 (br, 5H, NH₂), 4.30–4.60 (q, 2H, CH₂), 1.30–1.60 (t, 3H, CH₃). MS: m/z (%) [M⁺] = 275.125 (100%).

2.3.3. Synthesis of the Model Compound 4

A mixture of the diamino monomer 3 (1.09 g, 4.00 mmol) and LiCl (1.00 g) (as a catalyst) in 20 mL N-methyl-2-pyrrolidone (NMP) was stirred in an ice bath under nitrogen and then a solution of benzoyl chloride (1.12 g, 8.00 mmol) in 8 mL NMP was added to the reaction mixture. The stirring was continued for 6 h at room temperature. The reaction mixture was poured into iced water (100 mL) (Scheme 2). A solid product was separated, filtered off, washed well with water, dried, and recrystallized from toluene as yellow crystals; yield: 85%; m.p.: 213–215 °C. Anal. Calcd. for C₂₆H₂₂N₆O₄: C, 64.72; H, 4.60; N, 17.42; O, 13.26 Found: C, 63.99; H, 4.39; N, 16.88. FT-IR (KBr, cm^{−1}): 3412 (N-H, amide), 1714 (C=O, ester) and 1666 (C=O, amide). ¹H NMR (400 MHz, DMSO-d₆): δ = 8.68 (s, 2H, NH amide), 8.10–7.54 (m, 15H, 14 Ar-H, 1NH), 4.32 (q, 2H, CH₂), 1.34 (t, 3H, CH₃); MS: m/z (%) [M⁺] = 482.21 (29%).

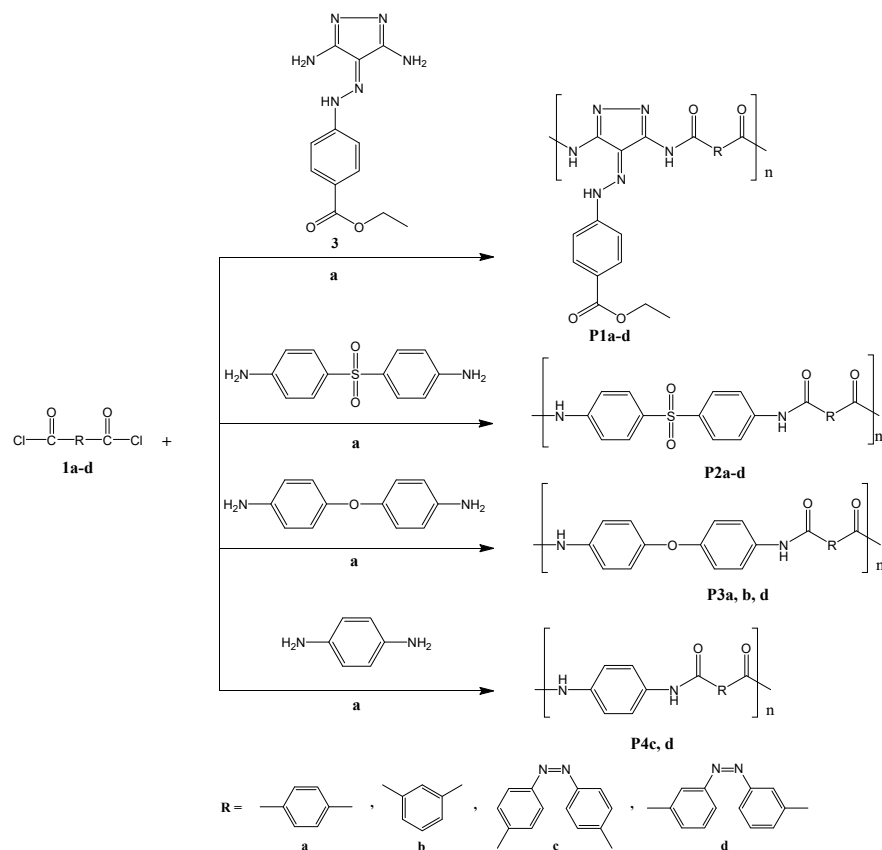


Scheme 2. Synthesis of model compound 4. Reagents and conditions: (a) LiCl anhydrous, NMP, N_2 , stirring, $-5\text{ }^\circ\text{C}$.

2.4. Polymers Syntheses

General Procedure A: For the Synthesis of Polyamides

A mixture of the diamino compound (4.00 mmol), and LiCl catalyst (1.00 g) in 20 mL NMP was stirred in an ice bath under nitrogen; then, a solution of diacid chloride (4.00 mmol) in 15 mL NMP was dropwise added while stirring over 20 min; the mixture was subsequently stirred for 6 h at room temperature. The reaction mixture was poured into iced water (Scheme 3). A solid polymer was separated, then washed with hot water and ethanol and dried under reduced pressure (1 mm/Hg) at $60\text{ }^\circ\text{C}$ for 24 h.



Scheme 3. Synthesis of polyamides P1a–d, P2a–d, P3a,b,d and P4c,d. Reagents and conditions: (a) LiCl anhydrous, NMP, N_2 , stirring, $-5\text{ }^\circ\text{C}$.

2.5. Synthesis of Iron Oxide Nanoparticles by Solvothermal Method

Fe_3O_4 NPs (Nanoparticles) were prepared by the solvothermal method. Teflon-lined stainless-steel autoclave was charged with a mixture of $\text{FeCl}_3 \cdot 6\text{H}_2\text{O}$ (0.5 gm), urea (1 gm), and citric acid (0.15 gm) in 60 mL of EG (Ethylene Glycol); then, the autoclave was sealed and maintained at $200\text{ }^\circ\text{C}$ for 20 h and finally cooled to room temperature. The Fe_3O_4

NPs were filtered off from the reaction mixture, then washed with DIW (deionized water) and ethanol sequentially, and dried in an oven at 80 °C [42]. FT-IR (ν) (KBr, cm^{-1}): 575 (stretching vibration Fe-O), 1639 (O-H bending), and 3423 cm^{-1} (O-H stretching).

Preparation of Polyamide/Fe₃O₄/ITO Electrodes and Polyamide/ITO Electrodes

The polyamide/ITO electrodes were prepared to measure the conductivity of polyamides. A (0.001 g, 1 mg/1 mL) of the polyamide was dissolved in 1 mL NMP; then, the ITO electrode was immersed in this solution for 6 h, taken out, rinsed with DIW, and dried. To prepare polyamide/Fe₃O₄/ITO electrodes, Fe₃O₄/ITO electrodes were firstly prepared by the solvothermal method [42]. Secondly, the Fe₃O₄/ITO electrode was immersed in a solution of (0.001 g) of the polyamide, dissolved in 1 mL NMP for 6 h, rinsed with DIW and dried.

2.6. Electrochemical Measurements

All the electrochemical measurements were performed under ambient laboratory conditions using the electrochemical workstation Metrohm (AUTOLAB) (Netherlands) instrument (Faculty of Science-Assiut University, Egypt) by using Ag/AgCl as a reference electrode, the polymer/Fe₃O₄/ITO electrode (1 cm × 1 cm) as a working electrode, and Pt as a counter electrode, based on cyclic voltammetry (CV) technique. All the used working electrodes were fabricated under the same conditions. The active geometrical area of the working electrode was 1 cm^2 ; the electrolyte volume was 20 mL; and the scan rate was 50 mV/s.

3. Results and Discussion

3.1. Monomer Synthesis

The diamino monomer **3** was synthesized in good yield by the reaction of one mole of the dicyano compound **2** with 1.1 moles of hydrazine hydrate, as described in Scheme 1. The chemical structures of the synthesized dicyano compound **2** and the diamino monomer **3** were confirmed via elemental analysis and spectral data. The FT-IR spectra displayed new characteristic absorption bands at 2230 cm^{-1} (CN) for the dicyano compound **2** and displayed characteristic absorption bands at 3300 & 3390 cm^{-1} (NH₂) for the diamino monomer **3** (see supporting information).

3.2. Synthesis of the Model Compound **4**

Before attempting the polymerization process, model compound **4** was synthesized by the reaction of one mole of diamino monomer **3** with two moles of benzoyl chloride in NMP using anhydrous LiCl as a catalyst under nitrogen, as described in Scheme 2. The chemical structure of the synthesized model compound was confirmed via elemental analysis and spectral data. The FT-IR spectrum of the model compound displayed characteristic absorption bands at 1714, and 1666 cm^{-1} due to (C=O ester) and (C=O, amide), respectively (see Supporting Information).

3.3. Polymerization and Polymer Characterization

The target four new series of polyamides P1a–d, P2a–d, P3a,b,d, and P4c,d, were synthesized using the polycondensation technique [43] by the interaction of one mole from the diamines with one mole of the dicarboxylic acid chlorides, as illustrated in Scheme 3. Polyamides P3c, P4a, and P4b were synthesized at a very low yield. The FT-IR spectra of all synthesized polyamides showed new characteristic bands at 1640–1690 cm^{-1} for (C=O, amide) and 3200–3460 cm^{-1} for (N-H, amide) groups, along with the presence of other characteristic absorption bands for specific groups present in the various polymers (see Supporting Information). Additionally, the ¹H NMR spectra of all polyamides in DMSO were compatible with the proposed structures (see Supporting Information). The various characteristics of the prepared polymers, including solubility, X-ray diffraction analysis, TGA, SEM, and electrochemical study with Fe₃O₄ nanoparticles, were determined, and all the data are discussed below.

3.3.1. Solubility

The solubility of all the synthesized polyamides P1a–d, P2a–d, P3a,b,d, and P4c,d was tested at room temperature using various solvents, including dimethylformamide (DMF), dimethylsulfoxide (DMSO), tetrahydrofuran (THF), chloroform, dichloromethane (DCM), N-methyl-2-pyrrolidone (NMP), and formic acid. A 0.5% (*w/v*) solution was taken as the criterion for solubility; the solution was then analyzed by visual inspection (see Table 1). All polymers are completely soluble in NMP and insoluble in CHCl₃ and DCM. It was noticed that the polymers in the first series, P1a–d, were slightly more soluble than in the other series. This behavior could be attributed to the steric hindrance effect of the substituted phenyl rings in polyamides P1a–d, which increases the chain packing distances, decrease the inter-chain interactions like hydrogen bonding, and thereby makes solvation easier [44].

Table 1. Solubility characteristics of the polyamides P1a–d, P2a–d, P3a,b,d, and P4c,d.

Polymer Code	DMF	DMSO	THF	CHCl ₃	DCM	HCOOH	NMP
P1a	+	+	+	-	-	+	++
P1b	+	+	+	-	-	+	++
P1c	+	+	+	-	-	+	++
P1d	+	+	+	-	-	+	++
P2a	+	+	-	-	-	+	++
P2b	++	++	+	-	-	-	++
P2c	+	+	-	-	-	-	++
P2d	-	+	-	-	-	-	++
P3a	-	+	-	-	-	-	++
P3b	-	++	-	-	-	-	++
P3d	-	+	-	-	-	-	++
P4c	-	+	+	-	-	-	++
P4d	-	++	+	-	-	-	++

3.3.2. X-ray Analysis

The X-ray diffractograms of the prepared polyamides P1a–d, P2a–d, P3a,b,d, and P4c,d available in the Supporting Information, showed a few reflection peaks intermediate between crystalline and amorphous phases in region $2\theta = 5\text{--}80^\circ$. This indicates that there is a large class of structures in the ordered states between crystalline and amorphous phases (with a pronounced long-range order) in the arrangement of their atoms and molecules [45,46]. Polyamides P1a, P1b, P2b, P2c, and P2d showed amorphous characters (i.e., no reflection sharpness peaks), while, in the polyamides P1c, P1d, P2a, P3a, P3d, P4c, and P4d, the reflection sharpness increased, and the polymers became semicrystalline. The presence of polar and hydrogen bonding groups in the polymer main chains increases the possibility of dipole–dipole and hydrogen bonding intermolecular forces, which increase the crystallinity of these polymers [47].

3.3.3. Scanning Electron Microscope (SEM) Measurements

The morphology of selected examples from the polyamides P1a, P1c, P2a, P2c, P3a, P3d, and P4c were examined by SEM using a low-dose technique [48]. The tested polymer samples were prepared as mentioned in the experimental section. Figure 1a (X = 2000) showed that polyamide P1a has a sponge shape with big pores; higher magnification (X = 5000) (Figure 1b) showed a cavity shape. Figure 1c,d (X = 2000 & 5000) showed that polyamide P1c has a spongy shape at different magnifications. Figure 1e (X = 2000) showed that polyamide P2a has a cavity shape with big pores; higher magnification (X = 10,000) (Figure 1f) showed a sub-globular structure. Figure 1g (X = 2000) showed that polyamide P2c has a spongy shape with big pores; higher magnification (X = 10,000) (Figure 1h) showed a cauliflower structure. Figure 1i,j (X = 2000 & 5000) showed that polyamide P3a has aggregates of layers structure at different magnifications. Figure 1k,l (X = 5000 & 10,000) showed that polyamide P3d has a spongy structure at different magnifications. It is worth

noting that the formed polymers showed non-uniform particle size, which means it is difficult to obtain the average particle size. ij153 software was used to study the particle sizes of the fabricated polymers. Twenty-five particles were selected randomly from each SEM image to calculate the average particle size. The distribution of the particle sizes of each polymer is represented in Supplementary Data. The average particle size of the P1a, P1c, P2a, P2c, P3a, and P3d was 640.000 nm, 512.192 nm, 268.651 nm, 203.978 nm, 233.090 nm, and 191.535 nm, respectively. Furthermore, the morphology of the Fe₃O₄ NPs-modified ITO electrode was studied using SEM. Figure 2 shows the SEM image of the Fe₃O₄ NPs-modified ITO electrode, which indicated the formation of nanoparticles.

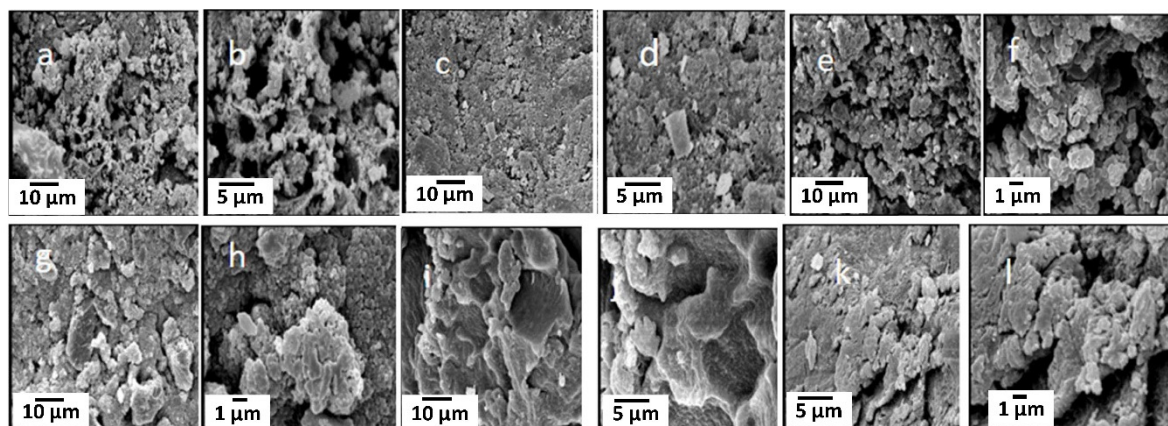


Figure 1. SEM images of polyamide surface at different magnifications; P1a (a) X = 2000, (b) X = 5000; P1c (c) X = 2000, (d) X = 5000; P2a (e) X = 2000, (f) X = 10,000; P2c (g) X = 2000, (h) X = 10,000; P3a (i) X = 2000, (j) X = 5000; P3d (k) X = 5000, (l) X = 10,000.

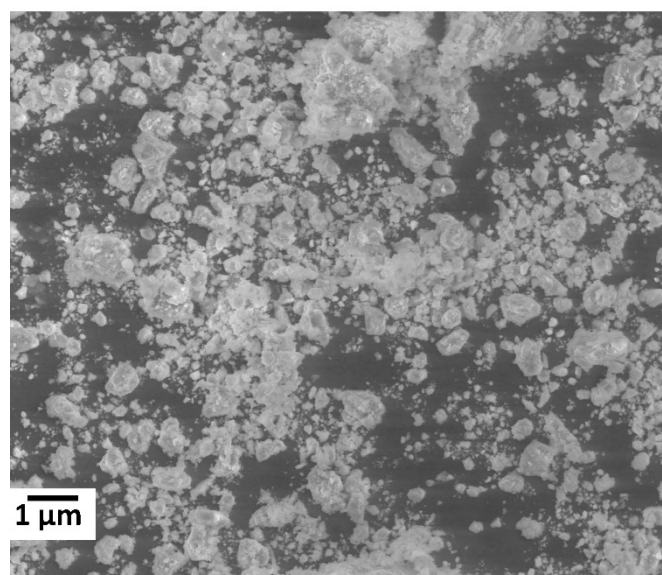


Figure 2. SEM image of Fe₃O₄/ITO electrode.

3.3.4. UV-Vis Absorption Study

The electronic absorption (UV-vis) of the polyamides P1a–d, P2a–d, P3a,b,d, and P4c,d were measured in NMP at (0.125 mg/mL) concentration at room temperature. The UV-vis spectra of all polyamides showed absorption bands at λ_{\max} 297–419 nm, due to the π - π^* transition within the benzenoid system and n - π^* transition of C=O groups, in addition to the extended conjugation in the polymers' main chains. In addition, the polymers P2c,d

showed absorption bands with λ_{\max} near 360–365 nm, which was attributed to the presence of the N=N group in the polymer backbone [49–52] (Figure 3).

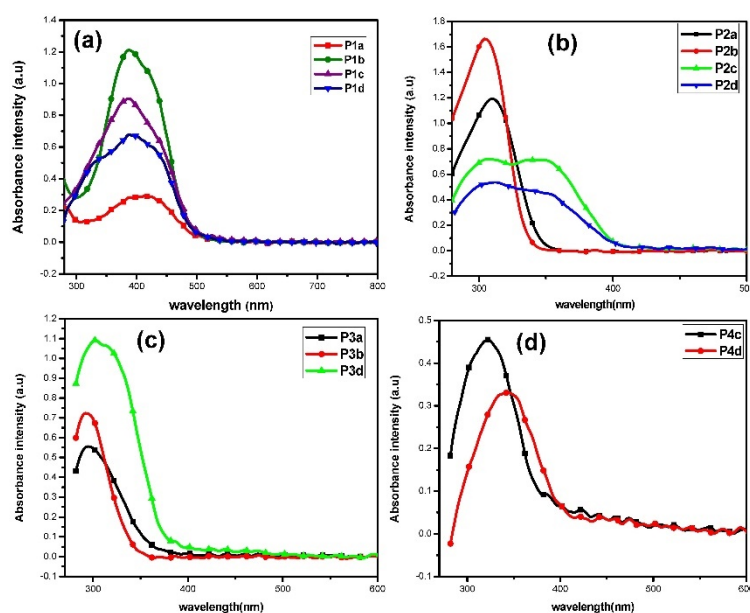


Figure 3. UV-vis absorption spectra of (a) P1a–d, (b) P2a–d, (c) P3a,b,d, and (d) P4c,d.

3.3.5. TGA Studies

The thermal behavior of all synthesized polyamides, P1a–d, P2a–d, P3a,b,d, and P4c,d, was evaluated by TGA under a nitrogen atmosphere at a heating rate of 10 °C/min (see Supporting Information). The temperature values, corresponding to 10%, 20%, 30%, 40%, and 50% weight loss in addition to char yield and LOI (limiting oxygen index) at 800 °C, are shown in Table 2. TGA curves showed a small weight loss within the range of 0.5 to 5%, starting at 49–290 °C, which may be attributed to the loss of moisture and trapped solvents [53]. TGA curves showed the initial decomposition temperature (IDT) of these polyamides (10% weight loss), which is the start of polymer decomposition and occurred within the range of 150 to 305 °C for all polyamides [54,55]. The temperature value of 50% weight loss ($T_{50\%}$) is one of the main criteria for determining the relative thermal stability of a polymer [56,57], which occurred within the range of 630 °C to 800 °C for these polyamides (see supporting information). The high thermal resistance of these aromatic polyamides, with decomposition temperatures above 500 °C, is a result of high-bond dissociation energies of C–N and C–C bonds [11]

Some of these polyamides, P1b, P2a, P2d, P3d, P4c, and P4d, showed one broad degradation step in their decomposition patterns, while, in the case of polyamides P1a, P1c, P1d, P2b, P2c and P3b, two degradation steps were observed, and the curves of some of these are slightly overlapped. P3a showed three overlapped degradation step curves.

The polyamide P1a showed mass loss between 195–430 °C (–15%) in the first region and mass loss between 430–640 °C (–23%) in the second region, also decomposing partially (residue at 800 °C was 52.50%). The polyamide P1b showed mass loss between 200–620 °C (–38%) in one region and decomposed partially (residue at 800 °C was 52.30%). The polyamide P1c showed mass loss between 155–270 °C (–13%) in the first region and mass loss between 270–615 °C (–25%) in the second region, also decomposing partially (residue at 800 °C was 52.90%). The polyamide P1d showed mass loss between 170–310 °C (–15%) in the first region and mass loss between 310–620 °C (–24%) in the second region, also decomposing partially (residue at 800 °C was 43.90%). The polyamide P2a showed mass loss between 305–750 °C (–40%) in one region and decomposed partially (residue at 800 °C was 51.00%). The polyamide P2b showed mass loss between 170–330 °C (–12%) in the first region and mass loss between 330–715 °C (–33%) in the second region, also decomposing

partially (residue at 800 °C was 44.70%). The polyamide P2c showed mass loss between 170–420 °C (−18%) in the first region and mass loss between 420–750 °C (−31%) in the second region, also decomposing partially (residue at 800 °C was 44.20%). The polyamide P2d showed mass loss between 150–710 °C (−44%) in one region and decomposed partially (residue at 800 °C was 47.00%). The polyamide P3a showed mass loss between 175–300 °C (−10%) in the first region, mass loss between 300–450 °C (−9%) in the second region, and mass loss between 450–750 °C (−35%) in the third region, also decomposing partially (residue at 800 °C was 41.30%). The polyamide P3b showed mass loss between 200–480 °C (−15%) in the first region and mass loss between 480–720 °C (−43%) in the second region, also decomposing partially (residue at 800 °C was 47.00%). The polyamide P3d showed mass loss between 280–715 °C (−35%) in one region and decomposed partially (residue at 800 °C was 52.70%). The polyamide P4c showed mass loss between 170–740 °C (−49%) in one region and decomposed partially (residue at 800 °C was 44.00%). The polyamide P4d showed mass loss between 180–750 °C (−51%) in one region and decomposed partially (residue at 800 °C was 41.50%).

Table 2. Thermal properties of the polyamides P1a–d, P2a–d, P3a,b,d and P4c,d.

Polyamide Code	Temperature (°C) for Various Decomposition Levels ^a							IDT ^b	(CR) ^c %	LOI ^d
	10%	20%	30%	40%	50%					
P1a	255	420	530	590	800	195	52.5	38.5		
P1b	310	450	536	596	800	200	52.4	38.46		
P1c	195	320	530	580	800	155	52.2	38.38		
P1d	225	412	531	594	767	170	51.5	38.10		
P2a	393	494	584	680	800	305	52.7	38.58		
P2b	253	403	560	648	737	170	44.2	35.18		
P2c	275	388	469	557	661	170	44.6	35.34		
P2d	235	297	390	500	690	150	48	36.7		
P3a	250	420	550	616	670	175	41.4	34.04		
P3b	305	480	550	610	680	200	47.4	36.46		
P3d	443	503	580	690	800	280	52.3	38.42		
P4c	210	300	398	500	660	170	44.2	35.18		
P4d	214	310	420	540	630	180	41.2	33.98		

^a: The values were determined by TGA at a heating rate of 10 °C min^{−1}. ^b: Initial decomposition temperature. ^c: The values of char residue. ^d: $LOI_{800^{\circ}C} = (17.5 + 0.4 CR)$, determined using Van Krevelan's equation.

As shown in Table 2, the LOI values of all prepared polyamides were calculated by using the char residue values obtained from TGA curves, according to Van Krevelen's equation ($LOI_{800^{\circ}C} = (17.5 + 0.4 CR)$) [58–60]. The LOI (limiting oxygen index) values of most polyamides (from 33.80 to 38.58) were higher than the limit value of 26, indicating that these polymers can be considered self-extinguishing materials.

The thermal cracking curve of P4a showed one broad degradation step. In this polymer, there are at least three possible positions where the fission can occur (as examples, see Supporting Information). Thus, the broad degradation step of this polymer could be attributed to the overlap between the degradation steps as the degradation temperatures of these steps are closed.

3.3.6. Qualitative Assessment of the Polymers' Conductivities

To shed more light on the conductivity of the prepared polyamides P1a–d, P2a–d, P3a,b,d, and P4c,d [61–63], they have been used to coat ITO electrodes. The thickness of the polymer layer was investigated using SEM. The standard SEM measurements provided

an indicative layer thickness of around 1–2 microns (see The Supplementary Material). The electrochemical conductivity of the prepared polyamide/ITO electrodes in $[\text{Fe}(\text{CN})_6]^{3-/4-}$ solution based on the CV technique [64–67], revealed that most of these prepared polyamide polymers are conducting polymers and most of them have higher conductivity than the bare ITO electrode (Figure S40a–d). The results indicated that the modification of the bare ITO with all prepared polyamide polymers led to enhancement of the electroconductivity, excepting three polymers (P2a, P2b, and P2d), which showed lower electrochemical conductivity compared with the bare ITO electrode.

3.3.7. Polyamides/ Fe_3O_4 NPs/ITO Electrodes for Analysis of MTX

To improve the electrochemical conductivity of the prepared polyamides, organic–inorganic hybrid polyamides/ Fe_3O_4 NPs/ITO electrodes were prepared. The formation of the organic–inorganic hybrids electrode was confirmed based on the XRD (Figure S37). Then, all the polyamides/ Fe_3O_4 NPs-modified ITO electrodes were applied for the MTX detection [68–70]. Figure 4 shows the CV responses of selected polyamides/ Fe_3O_4 NPs/ITO electrodes in the presence and the absence of 1 mM of MTX anticancer, which showed the highest CV response towards the MTX. Figure 4a shows the cyclic voltammograms of P3b/ Fe_3O_4 NPs/ITO in the presence and absence of 1 mM of MTX in PBS (pH = 7.4), which indicated the appearance of a broad cathodic peak at about -0.6 V and a strong and sharp oxidation peak at about -0.152 V. Furthermore, Figure 4b represents the cyclic voltammograms of P4d/ Fe_3O_4 NPs/ITO in the presence and the absence of 1 mM of MTX in PBS (pH = 7.4), which showed the appearance of a pair of sharp and strong redox peaks, including a cathodic peak at about -0.5 V and an oxidation peak at about -0.12 V. These results indicated that P4d/ Fe_3O_4 NPs/ITO electrode showed the highest electrochemical conductivity towards the MTX compared with bare ITO, Fe_3O_4 NPs/ITO and the rest of polyamides/ Fe_3O_4 NPs-modified ITO electrodes. Moreover, the low separation between the oxidation and reduction peaks in the case of the P4d/ Fe_3O_4 NPs/ITO electrode indicated that P4d/ Fe_3O_4 NPs/ITO electrode showed a more reversible response. The capability of the polyamides/ Fe_3O_4 NPs-modified ITO electrodes could be related to the presence of two carboxylic groups in the MTX moiety. The higher conductivity of the P4d/ Fe_3O_4 NPs/ITO electrode than the P3b/ Fe_3O_4 NPs/ITO electrode could be related to the short distance between the amino groups in the P3b compound than the P4d compound.

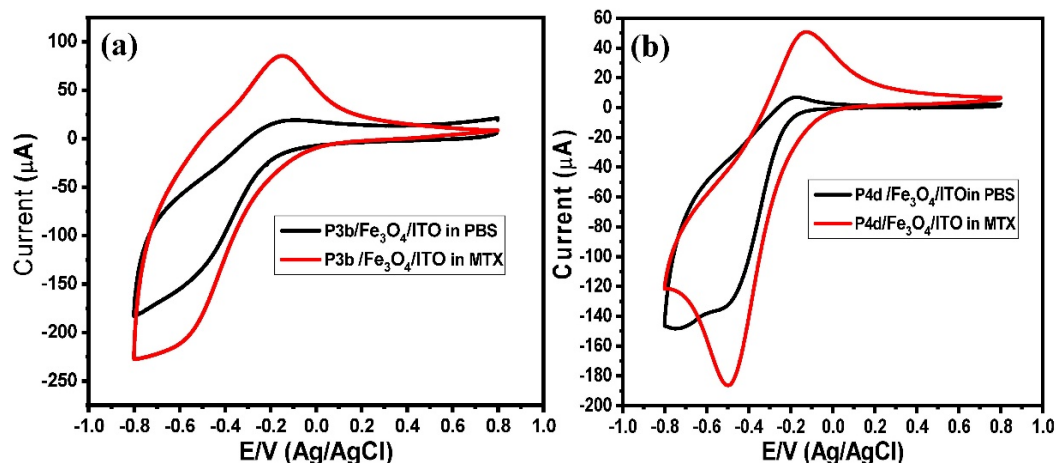


Figure 4. (a) CV of P3b/ Fe_3O_4 /ITO electrode in the buffer and MTX in buffer and 10^{-3} M MTX and (b) CV of P4d/ Fe_3O_4 /ITO electrode in buffer and 10^{-3} M MTX.

To study the stability of the developed polyamides/ Fe_3O_4 NPs-modified ITO electrodes towards the detection of MTX, P4d/ Fe_3O_4 /ITO electrode was used to detect MTX over 80 cycles. Figure 5a shows cyclic voltammograms of 10^{-9} mol L^{-1} of MTX at the P4d/ Fe_3O_4 /ITO electrode (80 cycles), which demonstrates that the intensity of the oxidation current peak was decreased with the cyclic numbers. The relationship between

the oxidation current peak and the cyclic number was studied. Figure 5b illustrates the relationship between the oxidation current peak (μA) and the cyclic number. Figure 5b demonstrates that the current peak decreased by about 25.6% of its value after 80 cycles, which means that the developed electrode retained about 74.5% of its conductivity after 80 cycles. These results indicated good stability after use for 80 cycles.

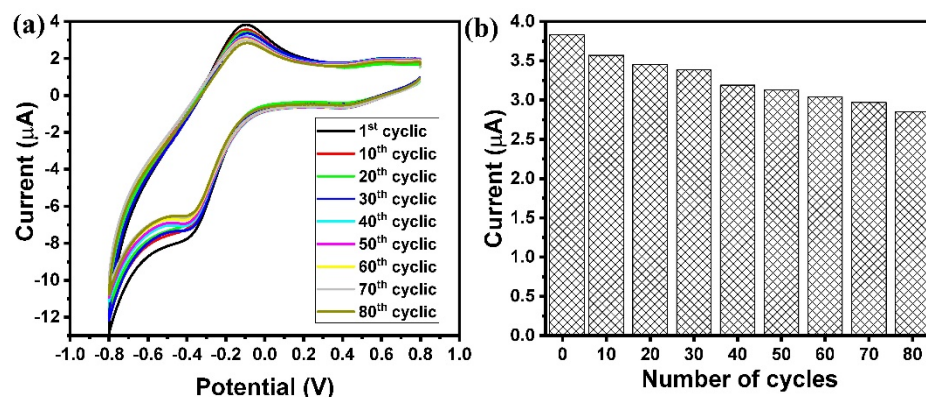


Figure 5. (a) Cyclic voltammograms of 10^{-9} mol L⁻¹ of MTX using P4d/Fe₃O₄/ITO electrode in PBS buffer pH = 7.4, scan rate = 50 mV/s, and (b) the calibration curve for the oxidation peak and the MTX concentrations.

Moreover, the sensitivity of the developed polyamides/Fe₃O₄ NPs-modified ITO electrodes towards the detection of MTX was also investigated. P4d/Fe₃O₄/ITO electrode was used to detect different a wide range of MTX concentrations. Figure 6a shows cyclic voltammograms of different MTX concentrations (10^{-9} : 10^{-14} mol L⁻¹) at the P4d/Fe₃O₄/ITO electrode, which demonstrated that the intensity of the oxidation current peak was increased with increasing the MTX concentration. The relationship between the oxidation current peak and the MTX concentration was studied. Figure 6b illustrated the relationship between the oxidation current peak (μA) and the logarithm (log) of the MTX concentration (nmol L⁻¹). The log function was used because of the very low values of the MTX concentrations (10^{-9} : 10^{-14} mol L⁻¹). Figure 6b demonstrates a linear curve within the MTX concentrations, from 10^{-9} to 10^{-14} mol L⁻¹ with an $R^2 = 0.9772$ and slope of 0.34 ± 0.03 . The calibration curve showed the ability of the developed sensor for detecting very low concentration values. The limit of detection of the developed sensor was found to be about 4.2 nmol L⁻¹.

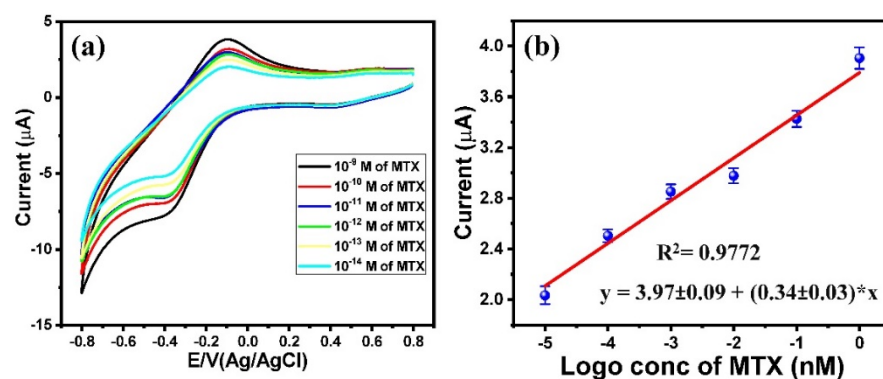


Figure 6. (a) Cyclic voltammetry of MTX using P4d/Fe₃O₄/ITO electrode at different concentration ranges from 10^{-9} to 10^{-14} M MTX in PBS buffer pH = 7.4, scan rate = 0.05 V/s; (b) the calibration curve for the oxidation peak and the MTX concentrations.

4. Conclusions

Here, we reported on the design, synthesis, and characterization of some new aromatic polyamides. The synthesized compounds were used to enhance the electrochemical

conductivity of the Fe₃O₄ NPs/ITO electrode. Some of these polyamides/Fe₃O₄ NPs/ITO electrodes showed higher electrochemical conductivity compared with the bare Fe₃O₄ NPs/ITO electrode. The polyamides-modified Fe₃O₄ NPs/ITO electrodes were used as electrochemical sensors for the determination of an anticancer drug, Methotrexate. The results demonstrated that the P3b/Fe₃O₄ NPs/ITO and P4d/Fe₃O₄ NPs/ITO electrodes revealed a good sensitivity toward the detection of Methotrexate. Thus, these electrodes represent a promising and less expensive method for monitoring Methotrexate.

Supplementary Materials: The following supporting information can be downloaded at: <https://www.mdpi.com/article/10.3390/surfaces6010007/s1>.

Author Contributions: Conceptualization, M.A.A.-R., W.A.E.-S. and A.-M.A.A.-W.; methodology, M.A.A.-R., W.A.E.-S. and E.M.S.; software, M.A.A.-R. and W.A.E.-S.; data curation, M.A.A.-R., E.M.S. and W.A.E.-S.; writing—original draft preparation, M.A.A.-R., W.A.E.-S., E.M.S. and A.-M.A.A.-W.; writing—review and editing, M.A.A.-R., W.A.E.-S. and A.-M.A.A.-W.; supervision, M.A.A.-R., W.A.E.-S. and A.-M.A.A.-W. All authors have read and agreed to the published version of the manuscript.

Funding: This research received no external funding.

Data Availability Statement: The authors confirm that the data supporting the findings of this study are available within the article and the supplementary data.

Acknowledgments: The Faculty of Science, Assiut University (Assiut, Egypt) is gratefully acknowledged for providing financial support and analytical instrumentation facility to carry out the research work.

Conflicts of Interest: The authors declare no conflict of interest.

References

1. Eggins, B.R. *Chemical Sensors and Biosensors*; John Wiley and Sons: UK, 2002.
2. Bănică, F.G. *Chemical Sensors and Biosensors: Fundamentals and Applications*, 1st ed.; John Wiley and Sons, Ltd.: West Sussex, UK, 2012.
3. Dincer, C.; Bruch, R.; Costa-Rama, E.; Fernández-Abedul, M.T.; Merkoçi, A.; Manz, A.; Urban, G.A.; Güder, F. Disposable Sensors in Diagnostics, Food, and Environmental Monitoring. *Adv. Mater.* **2019**, *31*, 1806739. [[CrossRef](#)]
4. Rodríguez-Mozaz, S.; Marco, M.; Lopez de Alda, M.J.; Barceló, D. Biosensors for environmental monitoring of endocrine disruptors. *Anal. Bioanal. Chem.* **2004**, *378*, 588–598.
5. Rodríguez-Mozaz, S.; Lopez de Alda, M.J.; Barceló, D. Biosensors as useful tools for environmental analysis and monitoring. *Anal. Bioanal. Chem.* **2006**, *386*, 1025–1041. [[CrossRef](#)] [[PubMed](#)]
6. Wang, J. Electrochemical Biosensors: Towards Point-Of-Care Cancer Diagnostics. *Biosens. Bioelectron.* **2006**, *21*, 1887–1892. [[CrossRef](#)] [[PubMed](#)]
7. Batool, R.; Rhouati, A.; Nawaz, M.H.; Hayat, A.; Marty, J.L. A Review of the Construction of Nano-Hybrids for Electrochemical Biosensing of Glucose. *Biosensors* **2019**, *9*, 46. [[CrossRef](#)] [[PubMed](#)]
8. Ermakov, V.; Kruchinin, S.; Fujiwara, A. Electronic nanosensors based on nanotransistor with bistability behaviour. In *Electron Transport in Nanosystems*; Bonca, J., Kruchinin, S., Eds.; Springer: Berlin, Germany, 2008; pp. 341–349.
9. Boric, A.; Kalendová, A.; Urbanek, M.; Pepelnjak, T. Characterisation of Polyamide (PA) 12 Nanocomposites with Montmorillonite (MMT) Filler Clay Used for the Incremental Forming of Sheets. *Polymers* **2019**, *11*, 1248. [[CrossRef](#)]
10. Anisio da Paz, R.; Leite, A.M.D.; Araújo, E.M.; Medeiros, V.; Alves de Melo, T.J.; Pessan, L.A. Mechanical and thermo mechanical properties of polyamide 6/Brazilian organoclay nanocomposites. *Polímeros* **2016**, *26*, 52–60.
11. Trigo-López, M.; Sanjuán, A.M.; Mendía, A.; Muñoz, A.; García, F.C.; García, J.M. Heteroaromatic Polyamides with Improved Thermal and Mechanical Properties. *Polymers* **2020**, *12*, 1793. [[CrossRef](#)]
12. Dahiya, J.B.; Muller-Hagedorn, M.; Bockhorn, H.; Kandola, B.K. Synthesis and thermal behaviour of polyamide 6/bentonite/ammonium polyphosphate composites. *Polym. Degrad. Stab.* **2008**, *93*, 2038–2041. [[CrossRef](#)]
13. Chen, G.; Wu, D.; Weng, W.; Yan, W. Preparation of Polymer/Graphite Conducting Nanocomposite by Intercalation Polymerization. *J. Appl. Polym. Sci.* **2001**, *82*, 2506–2513. [[CrossRef](#)]
14. Wu, H.; Krifa, M.; Koo, J.H. Flame retardant polyamide 6/nanoclay/intumescent nanocomposite fibers through electrospinning. *Text. Res. J.* **2014**, *84*, 1106–1118. [[CrossRef](#)]
15. Zhou, Y.-T.; Huang, Z.-Z.; Song, C.; Tang, C.-C.; Liu, X.-L.; Sheng, S.-R. New fluorinated aromatic polyamides based on N,N-bis(4-carboxyphenyl)-4-trifluoromethylaniline. *High Perform. Polym.* **2019**, *31*, 613–622. [[CrossRef](#)]
16. Horrocks, R.; Sitpalan, A.; Zhou, C.; Kandola, B.K. Flame Retardant Polyamide Fibres: The Challenge of Minimising Flame Retardant Additive Contents with Added Nanoclays. *Polymers* **2016**, *8*, 288. [[CrossRef](#)]

17. Majka, T.M.; Leszczyńska, A.; Kandola, B.K.; Pornwannachai, W.; Pielichowski, K. Modification of organo-montmorillonite with disodium H-phosphonate to develop flame retarded polyamide 6 nanocomposites. *Appl. Clay. Sci.* **2017**, *139*, 28–39. [[CrossRef](#)]
18. He, W.; Zhu, H.; Xiang, Y.; Long, L.; Qin, S.; Yu, J. Enhancement of flame retardancy and mechanical properties of polyamide 6 by incorporating an aluminum salt of diisobutylphosphinic combined with organoclay. *Polym. Degrad. Stab.* **2017**, *144*, 442–453. [[CrossRef](#)]
19. Bandaru, A.K.; Chouhan, H.; Bhatnagar, N. High strain rate compression testing of intra-ply and inter-ply hybrid thermoplastic composites reinforced with Kevlar/basalt fibers. *Polym. Test.* **2020**, *84*, 106407. [[CrossRef](#)]
20. Lingesb, B.V.; Ravikumar, B.N.; Rudresh, B.M. Investigation on the Mechanical Behavior of Polyamide 66/Polypropylene Blends. *Indian J. Adv. Chem. Sci.* **2016**, *4*, 168–171.
21. Oh, J.-H.; Bae, J.-H.; Kim, J.-H.; Lee, C.S.; Lee, J.-M. Effects of Kevlar pulp on the enhancement of cryogenic mechanical properties of polyurethane foam. *Polym. Test.* **2019**, *80*, 106093. [[CrossRef](#)]
22. Liang, Y.; Xia, X.; Lou, Y.; Jia, Z. Synthesis and performances of Fe₂O₃/PA-6 nanocomposite fiber. *Mater. Lett.* **2007**, *61*, 3269–3272. [[CrossRef](#)]
23. Gutch, P.K.; Banerjee, S.; Jaiswal, D.K. Synthesis and Properties of Novel Aromatic Polyamides Derived from 2,2-Bis[4-(4-amino-2-fluorophenoxy)phenyl]hexafluoropropane and Aromatic Dicarboxylic Acids. *J. Appl. Polym. Sci.* **2003**, *89*, 691–696. [[CrossRef](#)]
24. Soygun, K.; Bolayir, G.; Boztug, A. Mechanical and thermal properties of polyamide versus reinforced PMMA denture base materials. *J. Adv. Prosthodont.* **2013**, *5*, 153–160. [[CrossRef](#)]
25. Alaghemandi, M.; Gharib-Zahedi, M.R.; Spohr, E.; Böhm, M.C. Thermal conductivity of polyamide-6,6 in the vicinity of charged and uncharged graphene layers: A Molecular Dynamics Analysis. *J. Phys. Chem. C* **2012**, *116*, 14115–14122. [[CrossRef](#)]
26. Shoji, B.Y.; Mizoguchi, K.; Ueda, M. Synthesis of aramids by polycondensation of aromatic dicarboxylic acids with aromatic diamines containing ether linkages. *Polym. J.* **2008**, *40*, 680–681. [[CrossRef](#)]
27. Yao, J.; You, Y.; Lei, Y.; Dong, L.; Xiong, C.; Sun, Z. Main chain azo polyaramides with high thermal stability and liquid crystal properties. *J. Polym. Res.* **2009**, *16*, 455–460. [[CrossRef](#)]
28. He, L.; Mao, H.; Chao, D.; Zhany, W. Electroactive azo polyamide based oligoaniline: Synthesis and characterization. *Polym. J.* **2007**, *39*, 1172–1176. [[CrossRef](#)]
29. Choi, J.H.; Kim, T.H.; El-Said, W.A.; Lee, J.H.; Yang, L.; Conley, B.; Choi, J.W.; Lee, K.B. In Situ Detection of Neurotransmitters from Stem Cell-Derived Neural Interface at the Single-Cell Level via Graphene-Hybrid SERS Nanobiosensing. *Nano Lett.* **2020**, *20*, 7670–7679. [[CrossRef](#)] [[PubMed](#)]
30. Khan, F.; Akhtar, N.; Jalal, N.; Hussain, I.; Szmigielski, R.; Hayat, M.Q.; Ahmad, H.B.; El-Said, W.A.; Yang, M.; Janjua, H.A. Carbon-dot wrapped ZnO nanoparticle-based photoelectrochemical sensor for selective monitoring of H₂O₂ released from cancer cells. *Microchim. Acta* **2019**, *186*, 127. [[CrossRef](#)] [[PubMed](#)]
31. El-Said, W.A.; Kim, T.H.; Chung, Y.H.; Choi, J.W. Fabrication of New Single Cell chip to Monitor Intracellular and Extracellular Redox State based on Spectroelectrochemical method. *Biomaterials* **2015**, *40*, 80–87. [[CrossRef](#)] [[PubMed](#)]
32. Kim, T.H.; El-Said, W.A.; Choi, J.W. Highly Sensitive Electrochemical Detection of Potential Cytotoxicity of CdSe/ZnS Quantum Dots Using Neural Cell Chip. *Biosens. Bioelectron.* **2012**, *32*, 266–272. [[CrossRef](#)]
33. Rebollar-Pérez, G.; Campos-Terán, J.; Ornelas-Soto, N.; Méndez-Albores, A.; Torres, E. Biosensors based on oxidative enzymes for detection of environmental pollutants. *Biocatalysis* **2015**, *1*, 118–129. [[CrossRef](#)]
34. Khalid, M.; Mohammad, F. Preparation, electrical properties and thermal stability of conductive polyaniline: Nylon-6, 6 composite films. *eXPRESS Polym. Lett.* **2007**, *1*, 711–716. [[CrossRef](#)]
35. Arboleda-Clemente, L.; Ares-Pernas, A.; Garcia, X.; Dopico, S.; Abad, M.J. Improving the electrical properties of polyamide nanocomposites. *Soc. Plast. Eng.* **2016**, *1*, 1–3.
36. Meincke, O.; Kaempfer, D.; Weickmann, H.; Friedrich, C.; Vathauer, M.; Warth, H. Mechanical properties and electrical conductivity of carbon-nanotube filled polyamide-6 and its blends with acrylonitrile/butadiene/styrene. *Polymer* **2004**, *45*, 739–748. [[CrossRef](#)]
37. Yan, D.; Zhang, H.B.; Jia, Y.; Hu, J.; Qi, X.Y.; Zhang, Z.; Yu, Z.Z. Improved electrical conductivity of polyamide 12/grapheme nanocomposites with maleated polyethylene-octene rubber prepared by melt compounding. *ACS Appl. Mater. Interfaces* **2012**, *4*, 4740–4745. [[CrossRef](#)]
38. Zhou, S.; Chen, Y.; Zou, H.; Liang, M. Thermally conductive composites obtained by flake graphite filling immiscible polyamide 6/polycarbonate blends. *Thermochim. Acta* **2013**, *566*, 84–91. [[CrossRef](#)]
39. Kim, T.D.; Bae, H.M.; Lee, K.S. Synthesis and characterization of a new polyester having photo-crosslinkable cinnamoyl group. *Bull. Korean Chem. Soc.* **2002**, *23*, 1031–1034.
40. Sanadhya, S.G.; Oswal, S.; Parmar, K.C. Synthesis and characterization of wholly aromatic polyesters using interfacial polycondensation technique. *Der Pharma Chem.* **2014**, *6*, 156–163.
41. Gorde, P.; Pingle, A.; Wagh, S. Design and development of novel azobenzene dicarboxylic acid allyl ester polymers for colon specific drug delivery. *IJPR* **2014**, *5*, 1491–1498.
42. El-Said, W.A.; Abdel-Rahman, M.A.; Sayed, E.M.; Abdel-Wahab, A.A. Electrochemical Monitoring of Methotrexate Anticancer Drug in Human Blood Serum by Using in situ Solvothermal Synthesized Fe₃O₄/ITO Electrode. *Electroanalysis* **2019**, *31*, 829–837. [[CrossRef](#)]
43. Aly, K.I.; Abdel-Rahman, M.A.; Hussein, M.A. New polymer syntheses Part 53. Novel polyamides of diarylidene cycloalkane containing azo groups in the polymer backbone: Synthesis and characterization. *Int. J. Polym. Mater.* **2010**, *59*, 553–569. [[CrossRef](#)]
44. Hammam, A.S.; Aly, K.I.; Radwan, S.M.; Abdel-Rahman, M.A. Liquid crystalline polymers VIII: Thermotropic liquid crystalline poly(hydrazone-ether)s containing bis-thiophene linked to the main chain through spacers of various lengths. *J. Sulfur Chem.* **2007**, *28*, 547–561. [[CrossRef](#)]

45. Aly, K.I.; Hammam, A.S.; Radwan, S.M.; Abdel-Rahman, M.A. New Unsaturated Copolyesters based on Diarylidene-cyclopentanone. Optimum conditions of Synthesis, Characterization and Morphology. *Int. J. Bas. Appl. Sci.* **2010**, *11*, 15–35.
46. Aly, K.I.; Al-Muaiikel, N.S.; Abdel-Rahman, M.A.; Tolba, A.H. Liquid crystalline polymers XVI. Thermotropic liquid crystalline copoly(arylidene-ether)/TiO₂ Nanocomposites: Synthesis, characterisation and applications. *Liq. Cryst.* **2019**, *46*, 1734–1746. [[CrossRef](#)]
47. Ebewele, R.O. Chemical bonding and polymer structure, morphology of crystalline polymers. In *Polymer Science and Technology*; CRC Press: Boca Raton, NY, USA, 2000; Chapter 3; pp. 90–107.
48. Tager, A. *Physical Chemistry of Polymers*; Mir Publisher: Moscow, Russia, 1972; pp. 303–310.
49. Hsiao, S.H.; Peng, S.C.; Kung, Y.R.; Leu, C.M.; Lee, T.M. Synthesis and electro-optical properties of aromatic polyamides and polyimides bearing pendent 3,6-dimethoxycarbazole units. *Eur. Polym. J.* **2015**, *73*, 50–64. [[CrossRef](#)]
50. Bundgaard, E.; Krebs, F.C. Low band gap polymers for organic photovoltaics. *Sol. Energy Mater. Sol. Cells* **2007**, *91*, 954–985. [[CrossRef](#)]
51. Agrawal, S.; Narula, A.K. Facile synthesis of new thermally stable and organosoluble polyamide-imides based on non-coplanar phosphorus and silicon containing amines. *J. Chem. Sci.* **2014**, *126*, 1849–1859. [[CrossRef](#)]
52. Hsiao, S.H.; Liou, G.S.; Kung, Y.C.; Hsiung, T.J. Synthesis and properties of new aromatic polyamides with redox-active 2,4-dimethoxytriphenylamine moieties. *J. Polym. Sci. Part A Polym. Chem.* **2010**, *48*, 3392–3401. [[CrossRef](#)]
53. Zhao, Z.P.; Guo, Q.; Li, X.; Sun, J.L.; Nie, Z.J. Synthesis and thermal degradation characterization of novel poly(phosphazene-aryl amides). *EXPRESS Polym. Lett.* **2012**, *6*, 308–317. [[CrossRef](#)]
54. Hussein, M.A.; Abdel Rahman, M.A.; Aly, K.I. New polymer syntheses part 56: Novel friedel-crafts polyketones containing naphthalene moiety: Synthesis, characterization and antimicrobial activity. *J. Macromol. Sci. Part A* **2013**, *50*, 99–109. [[CrossRef](#)]
55. Aly, K.I.; Abdel-Rahman, M.A.; Tolba, A.H. Liquid crystalline polymers XV. Synthesis, properties and cytotoxicity of photoresponsive thermotropic liquid crystalline copoly (arylidene-ether)s based on 4-tert-butylcyclohexanone and cyclohexanone moieties in the main chain. *Liq. Cryst.* **2018**, *45*, 187–203. [[CrossRef](#)]
56. Hussein, M.A.; Abdel-Rahman, M.A.; Geies, A.A. New heteroaromatic polyazomethines containing naphthyridine moieties: Synthesis, characterization, and biological screening. *J. Appl. Polym. Sci.* **2012**, *126*, 2–12. [[CrossRef](#)]
57. Rao, V.S.; Samui, A. Molecular engineering of photoactive liquid crystalline polyester epoxies containing benzylidene moiety. *J. Polym. Sci. Part A Polym. Chem.* **2008**, *46*, 7637–7655. [[CrossRef](#)]
58. Kiziltas, E.E.; Yang, H.S.; Kiziltas, A.; Boran, S.; Ozen, E.; Gardner, D.J. Thermal analysis of polyamide 6 composites filled by natural fiber blend. *BioResources* **2016**, *11*, 4758–4769. [[CrossRef](#)]
59. Balaji, K.; Murugavel, S.C. Synthesis, spectral and thermal characterization of photosensitive poly(ether-ester)s containing α,β -unsaturated ketone moieties in the main chain derived from 2,6-bis[4-(3-hydroxypropyloxy)-3-methoxy-benzylidene]cyclohexanone. *J. Appl. Polym. Sci.* **2011**, *120*, 3141–3150. [[CrossRef](#)]
60. Muthusamy, A.; Balaji, K.; Murugavel, S.C. Synthesis, thermal, and photocrosslinking studies of thermotropic liquid crystalline poly(benzylidene-ether) esters containing α,β -unsaturated ketone moiety in the main chain. *J. Polym. Sci. Part A Polym. Chem.* **2013**, *51*, 1707–1715. [[CrossRef](#)]
61. Gorrasi, G.; Bredeau, S.; Candia, C.; Patimo, G.; De Pasquale, S.; Dubois, P. Electroconductive polyamide 6/MWNT nanocomposites: Effect of nanotube surface-coating by in situ catalyzed polymerization. *Macromol. Mater. Eng.* **2011**, *296*, 408–413. [[CrossRef](#)]
62. Hooshmand, S.; Soroudi, A.; Skrifvars, M. Electro-conductive composite fibers by melt spinning of polypropylene/polyamide/carbon nanotubes. *Synth. Met.* **2011**, *161*, 1731–1737. [[CrossRef](#)]
63. Park, S.C. Electroconductive polyamide resin composition and molded product for motor component prepared therefrom. U.S. Patent No. 6,828,375, 7 December 2004.
64. Wang, K.; Lin, X.; Zhang, M.; Li, Y.; Luo, C.; Wu, J. Review of Electrochemical Biosensors for Food Safety Detection. *Biosensors* **2022**, *12*, 959. [[CrossRef](#)]
65. Zhang, Y.; Lin, T.; Shen, Y.; Li, H. A High-Performance Self-Supporting Electrochemical Biosensor to Detect Aflatoxin B1. *Biosensors* **2022**, *12*, 897. [[CrossRef](#)]
66. Rong, Q.; Han, H.; Feng, F.; Ma, Z. Network nanostructured polypyrrole hydrogel/Au composites as enhanced electrochemical biosensing platform. *Sci. Rep.* **2015**, *5*, 11440. [[CrossRef](#)]
67. Cui, F.; Jafarishad, H.; Zhou, Z.; Chen, J.; Shao, J.; Wen, Q.; Liu, Y.; Zhou, H.S. Batch fabrication of electrochemical sensors on a glycol-modified polyethylene terephthalate-based microfluidic device. *Biosens. Bioelectron.* **2020**, *167*, 112521. [[CrossRef](#)] [[PubMed](#)]
68. Niu, L.M.; Lian, K.Q.; Shi, H.M.; Wu, Y.B.; Kang, W.J.; Bi, S.Y. Characterization of an ultrasensitive biosensor based on a nano-Au/DNA/nano-Au/poly (SFR) composite and its application in the simultaneous determination of dopamine, uric acid, guanine, and adenine. *Sens. Actuators B Chem.* **2013**, *178*, 10–18. [[CrossRef](#)]
69. Stefan, R.I.; Bokretsiou, R.G.; Frederick van Staden, J.; Aboul-Enein, H.Y. Simultaneous determination of L-and D-methotrexate using a sequential injection analysis/ampereometric biosensors system. *Biosens. Bioelectron.* **2003**, *19*, 261–267. [[CrossRef](#)] [[PubMed](#)]
70. Linting, Z.; Ruiyi, L.; Zaijun, L.; Qianfang, X.; Yinjun, F.; Junkang, L. An immunosensor for ultrasensitive detection of aflatoxin B1 with an enhanced electrochemical performance based on graphene/conducting polymer/gold nanoparticles/the ionic liquid composite film on modified gold electrode with electrodeposition. *Sens. Actuators B Chem.* **2012**, *174*, 359–365. [[CrossRef](#)]

Disclaimer/Publisher's Note: The statements, opinions and data contained in all publications are solely those of the individual author(s) and contributor(s) and not of MDPI and/or the editor(s). MDPI and/or the editor(s) disclaim responsibility for any injury to people or property resulting from any ideas, methods, instructions or products referred to in the content.